Interface-bonding Layer for Finite Element Analysis of Carbon Fiber Sheets Bonded to Concrete

Gabriel Sirbu*, Tamon Ueda**, Yoshio Kakuta***

*PhD candidate, Graduate School of Eng., Hokkaido University, Kita-ku, Sapporo, 060-8628
**Dr. of Eng., Associate Professor, Graduate School of Eng., Hokkaido University, Kita-ku, Sapporo, 060-8628
***Dr. of Eng., Professor, Graduate School of Eng., Hokkaido University, Kita-ku, Sapporo, 060-8628

Application of FRP strengthening methods on reinforced concrete members requires analytical tools capable to predict correctly the interfacial stresses developed between the concrete and the FRP composite material. The aim of this study is to develop finite elements for Carbon Fiber Sheet (CFS) composite bonded to reinforced concrete (RC) elements and the interface layer between the CFS composite and RC. Analytical results are presented in comparison with experimental ones. The developed finite elements can model the behaviour of the CFS composite and can predict with good accuracy not only peak pull-out force but also the level of strains and stresses observed in the experiments in both CFS composite and interface layer.

Key Words: Bond, Carbon Fiber Sheet, FEM, Interface layer

1. Research significance

Fiber reinforced plastics (FRP) have been used in strengthening reinforced concrete (RC) structures in the recent years. The properties like high tensile strength, lightweight and resistance to corrosion made the option of using them very attractive. Generally, the FRP materials are bonded using epoxy resins on the surface of the RC elements. Their mechanical properties vary with the orientation of the reinforcing fibers[1]. This allows the designer to increase the strength in any desired direction.

The performance of the strengthening FRP material depends on the capability of the interface-bonding layer to transfer the shear stresses from concrete to the FRP. The peeling failure was previously studied both experimentally and theoretically by many researchers[2), 3)]. In this paper the focus is placed on the failure mode governed by the shearing of the concrete next to the interface-bonding layer. The target of this research is to propose a suitable finite element modelling for the interface-bonding layer.

Most of the previous researchers presented a two-dimensional approach, in which one of the dimensions represented the thickness of the different materials modelled[3), 4)]. This approach allows analysis using finite element method (FEM) only for cases like beams strengthened with FRP composites attached at the lower part.

The present paper proposes a method that may be applied for the analysis of a cantilever beam or a column subjected to lateral forces, in which the FRP material is used as transverse reinforcement and is applied on the lateral surfaces of the member. In this case the FRP material is applied on the surface that is visible in the plane of analysis. The advantage of this method is that the thickness of the FRP material and RC are normal to the plane in which analysis is performed while the analysis still remains two-dimensional.

2. Constitutive model for interface-bonding layer

2.1 Previous research

Based on experimental measurement of strains in concrete-FRP samples using moiré interferometry, Y.-J. Lee et al.[5)] proposed a theoretical model. This model was based on linearity of slip and bond stress. It was concluded that the analytical results agreed with experimental results until a secondary crack occurred. After the formation of a secondary crack, the model did not agree anymore with the experimental results.

Using the results obtained on tests of FRP plates bonded to concrete, Michael J. Chajes et al.[6)] proposed an idealized model with the characteristics of a linearly decreasing strain distribution. The research provides important information about the bond mechanism and the influencing parameters like bond length and material properties, yet the authors concluded that additional experimental and analytical work is needed.

Yasuhiko Sato et al.[7)] proposed a method to calculate the ultimate load carried by a unidirectional FRP material bonded on concrete. The proposed equation was based on the effective bond length and the average bond stress observed in large range of experiments. While the results presented showed a good agreement between the predicted values and the observed ones, the author did not present a model that could be applied in a FEM program at that time.

J. Yin and Z.Wu[8)] used a model based on fracture energy for the two shear stress-slip relationships, which

they proposed. The relationships were implemented in a FEM program and a comparison with an FRP-strengthened beam was made. The model leaves the bond strength and the interfacial fracture energy as parameters.

2.2 Model in this study

Recently, Yasuhiko Sato et al.[9), 10)] presented an extended study of the bond mechanism of carbon fiber sheet (CFS). A model for bond stress-slip relationship was developed based on extensive experimental results of different tests using CFS bonded to concrete with epoxy resin. The presented FEM approach remains in the case where the thickness of the CFS is represented by one of the principal directions in the analysis plane.

Figure 1 shows the bond stress-slip relationship presented by Y. Sato et al in comparison with experimental results.

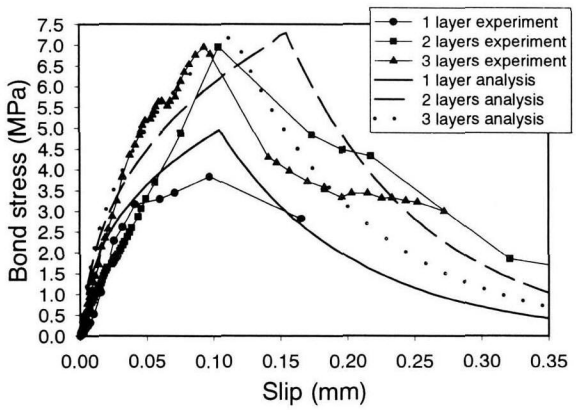

Fig.1 Bond stress-slip relationship [10)]

The bond stress-slip relationship can be expressed in a simplified manner as follows[10)]:

$$\tau = \frac{\tau_{\max}}{s_0} G_0 D^* s \tag{1}$$

before maximum bond stress and

$$\tau = \tau_{\max} \exp[-10(s - s_0)] \tag{2}$$

after maximum bond stress, where

$$\begin{aligned} s_0 &= 0.8 \times 10^{-12} (tE_{CFS})^{2.4} f_c'^{0.2} + 0.021 \\ G_0 &= 0.0936 (tE_{CFS})^{0.417} \end{aligned} \tag{3}$$

for tE_{CFS}>38.4 GPa, and

$$\begin{aligned} s_0 &= \frac{3100}{tE_{CFS}} f_c'^{0.2} + 0.034 \\ G_0 &= 1 + \frac{25500}{tE_{CFS}} \end{aligned} \tag{4}$$

for tE_{CFS}<38.4 GPa, and:

$$\tau_{\max} = 9.1 f_c'^{0.2} tE_{CFS} \times 10^{-5} \le 3.49 f_c'^{0.2} \quad 5)$$

In the above equations f_c' is the concrete compressive strength, τ is the bond stress, $\tau_{\max}$ is the maximum bond stress; t is the thickness of the CFS and E_{CFS} its stiffness along the fiber direction, s_0 is the slip corresponding to the maximum bond stress, s is the slip, G_0 has the significance of initial shear stiffness of the interface-bonding layer and D^* represents its degradation function defined as:

$$\begin{aligned} D^* &= 1 - \exp\left[\alpha \left(\frac{s}{s_0}\right)^{-\beta}\right] \\ \alpha &= \ln\left(1 - \frac{1}{G_0}\right) \\ \beta &= 0.2665 (tE_{CFS})^{0.083} \le 0.64 \end{aligned} \tag{6}$$

The units used in all equations are mm and MPa.

The original model is defined in a more complicated way. For easiness, the equations 1 to 6 were adopted for description of the model[10)] and applied in this study.

3. Finite element modelling for interface-bonding layer

Hajime Okamura and Koichi Maekawa originally developed the FEM program used by the authors, for nonlinear analysis of reinforced concrete[11)]. The program uses 8 nodes isoparametric elements for RC. The constitutive laws for CFS material and the bond stress-slip, presented in section 2.2, model for the interface layer, were implemented into the program. The CFS is modelled using also 8 nodes isoparametric elements. For the interface layer, a 16 nodes brick element is used.

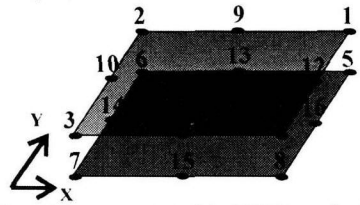

Fig.2 Elements used in FEM analysis

Figure 2 shows the way in which the CFS and the RC elements are used in this analysis. The nodes 5, 6, 7, 8, 13,14, 15 and 16 denote the RC element. The nodes 1, 2, 3, 4, 9, 10, 11, 12 denote the CFS element. The interface layer is defined using all the 16 nodes from the CFS and RC.

The stress vector in "XOY" system of coordinates for CFS element can be defined as follows:

$$\begin{Bmatrix} \sigma_X \\ \sigma_Y \\ \tau_{XY} \end{Bmatrix} = \begin{bmatrix} Q_{11} & Q_{12} & 0 \\ Q_{21} & Q_{22} & 0 \\ 0 & 0 & Q_{33} \end{bmatrix} \times \begin{Bmatrix} \varepsilon_X \\ \varepsilon_Y \\ \gamma_{XY} \end{Bmatrix} \tag{7}$$

where:

$$\begin{aligned} Q_{11} &= \frac{E_{11}}{(1 - \nu_{12}\nu_{21})} \\ Q_{22} &= \frac{E_{22}}{(1 - \nu_{12}\nu_{21})} \\ Q_{12} = Q_{21} &= \frac{\nu_{21} E_{11}}{(1 - \nu_{12}\nu_{21})} \end{aligned} \tag{8.a}$$

$$E_{11} = V_f E_{CFL} + (1 - V_f) E_m$$

$$E_{22} = \frac{E_{CFL} E_m}{(1 - V_f) E_{CFT} + V_f E_m}$$

$$\nu_{21} = \nu_{12} \frac{E_{22}}{E_{11}} \tag{8.b}$$

$$\nu_{12} = \nu_{CFL} V_f + \nu_m (1 - V_f)$$

$$Q_{33} = \frac{G_m \left[G_{CF} (1 + V_f) + G_m (1 - V_f) \right]}{\left[G_m (1 + V_f) + G_{CF} (1 - V_f) \right]}$$

In the above equations, E_{CFL} is the elastic modulus of carbon fiber along the fiber; E_{CFT} is the elastic modulus of the carbon fiber normal to the fiber direction; G_{CF} is the shear modulus of the carbon fiber; E_m represents the elastic modulus of the resin matrix; G_m the shear modulus of the resin matrix; ν_{CFL} the Poisson's ratio of the carbon fiber along the fiber direction; ν_m the Poisson's ratio of the resin matrix; V_f is the volume fraction of the fibres; E_{11} and E_{22} are the elastic modulus of the composite along the fiber direction and normal to it respectively; ν_{12} and ν_{21} corresponding Poisson's ratios.

The calculation of the stress vector of the interface element is carried out using the general stiffness matrix of an orthotropic material, given by:

$$\begin{Bmatrix} \sigma_X \\ \sigma_Y \\ \sigma_Z \\ \tau_{XY} \\ \tau_{YZ} \\ \tau_{XZ} \end{Bmatrix} = \begin{bmatrix} Q_{11} & Q_{12} & Q_{13} & 0 & 0 & 0 \\ Q_{21} & Q_{22} & Q_{23} & 0 & 0 & 0 \\ Q_{31} & Q_{32} & Q_{33} & 0 & 0 & 0 \\ 0 & 0 & 0 & Q_{44} & 0 & 0 \\ 0 & 0 & 0 & 0 & Q_{55} & 0 \\ 0 & 0 & 0 & 0 & 0 & Q_{66} \end{bmatrix} \times \begin{Bmatrix} \varepsilon_X \\ \varepsilon_Y \\ \varepsilon_Z \\ \gamma_{XY} \\ \gamma_{YZ} \\ \gamma_{XZ} \end{Bmatrix} \tag{9}$$

where:

$$Q_{11} = Q_{22} = Q_{33} = Q(1 - \nu_m)$$

$$Q_{12} = Q_{21} = Q_{13} = Q_{31} = Q_{23} = Q_{32} = Q\nu_m$$

$$Q_{44} = Q_{55} = Q_{66} = \frac{E_m}{2(1 + \nu_m)} \tag{10}$$

$$Q = \frac{E_m}{(1 + \nu_m)(1 - 2\nu_m)}$$

In order to obtain a compatible system of equations, the elements that are contributing to the calculation of the stress normal to the plane of analysis (σ_Z) are ignored.

Only the terms Q_{55} and Q_{66} have a nonlinear variation depending on the slip between the layer defined by the CFS element and the layer defined by the RC element. Eq. 10 gives the initial value for these two terms. Using a degradation function derived from Eqs. 1 to 6 the terms Q_{55} and Q_{66} are re-evaluated for each sampling point of the interface-bonding element at each loading step according to the magnitude of the maximum slip that was registered at the location of the sampling point during the loading history. The rest of the terms are kept constant. Figure 3 presents the shear stiffness degradation and slip relationship for different number of CFS layers derived from the bond stress and slip relationship plotted in Figure 1.

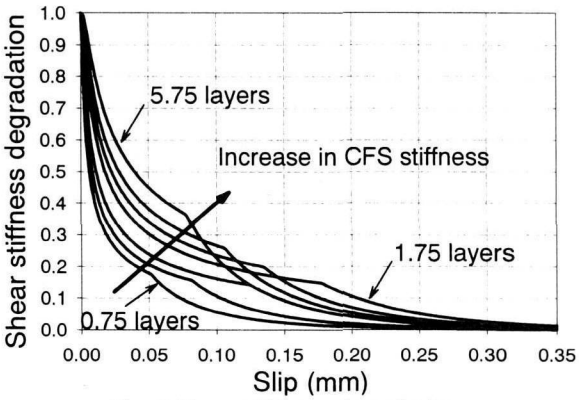

Fig. 3 Shear stiffness degradation

4. Validation of proposed modelling

The test specimens chosen for this study are selected from the specimens used by Y. Sakai[12] and W. Moriwaki[13]. Table 1 and Table 2 present the material characteristics for CFS and epoxy resin respectively (unit = GPa).

Table 1 CFS material characteristics

E_{CFL}	E_{CFT}	G_{CF}	ν_{CFL}
244.18	20.59	28.73	0.33

Table 2 Epoxy resin material characteristics

E_m	G_m	ν_m
2.21	0.80	0.38

Figure 4 presents the general test setup.

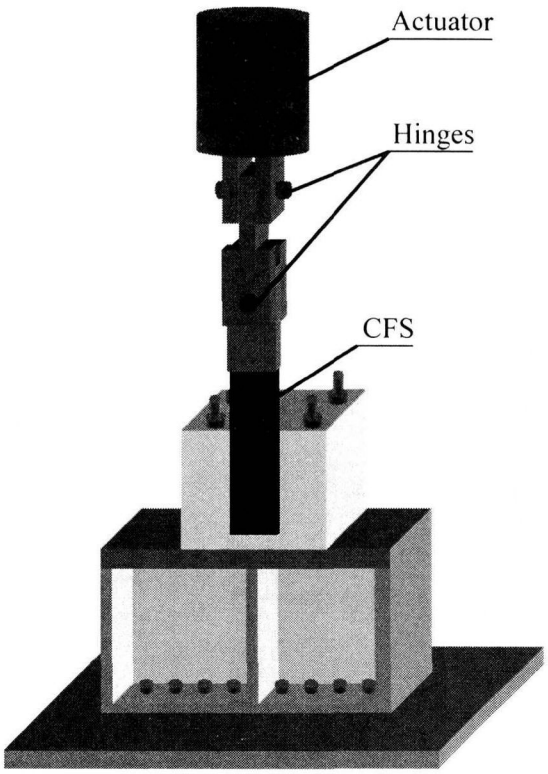

Fig. 4 Test setup

All specimens tested have the same bond width, equal to 100mm. The CFS composite was bonded on a lateral surface of a concrete block, leaving a 20mm unbonded zone from the edge of the face. Then, the unbonded end of the CFS composite was pulled until complete debonding was obtained. Table 3 presents the details of the test specimens.

Table 3 Details of specimens

Specimen	f'_c (MPa)	Nr. of CFS layers	Bond length (mm)	Ultimate load (kN)
S1L200	40.9	1	200	20.40
S3L200	39.6	3	200	46.73
S3L300	33.2	3	300	50.82
S5L200	45.2	5	200	45.68
S5L300	36.5	5	300	58.10

Figures 5 and 6 show the failure surface for specimens S1L200 and S5L300 after complete debonding from the concrete block. In all cases, the failure mode was complete debonding of the CFS composite due to the fracture of the concrete surface. The failure surface was obtained in the thin layer of concrete under the CFS composite. There is no difference in the failure modes between the specimens considered, whatever was the CFS composite stiffness (number of layers) or bonding length. It can be observed that in addition to the CFS bonded area the failure surface includes the adjacent zones because the epoxy resin was applied on a wider area. Figure 7 shows pictures of the cross-sections in the CFS composite (specimen S3L300) after complete debonding from the concrete block.

Similar cross-sections were obtained from the other specimens.

Fig. 5 S1L200 after complete debonding

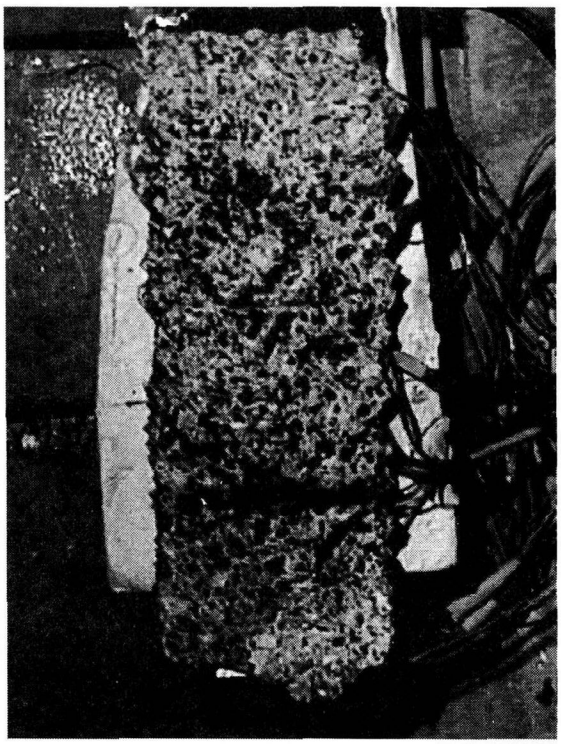

Fig. 6 S5L300 after complete debonding

The pictures were taken using a macro lens, and the cross-sections were cut at different locations normal to the fiber direction. The reference scale superposed on the pictures has the unit in mm.

From the investigation of the thickness of the different layers it was found that the thin layer of concrete which was peeled off from the concrete block has an average thickness of 2.5~3.0mm. In addition, it was found that the CFS composite thickness was not uniform all over the entire bonded surface. The small differences observed were caused by the fact that the epoxy resin that impregnates the carbon fibers was manually applied.

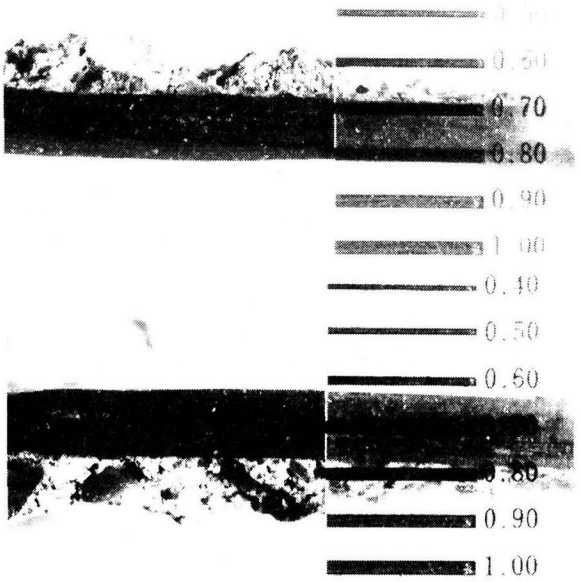

Fig. 7 S3L300 Cross-sections in CFS composite

4.2. Comparison between experiment and FEM results

The proposed method is verified by making the comparison between experimental and finite element analysis. Figure 8 shows the geometrical characteristics of the specimens used in this study and the way in which they were divided for FEM analysis. The general mesh used for analysis is shown in Figure 9.

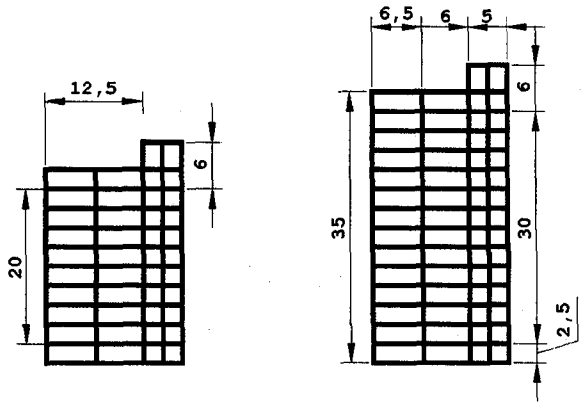

Fig. 8 Geometrical characteristics of the specimens (cm)

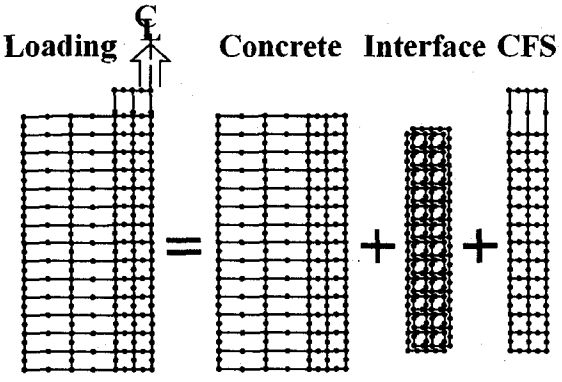

Fig. 9 General FEM model

Table 4 Average thickness values

Specimen	Material	Average thickness (mm)
S1L200	Bonded CFS	0.628
	Unbonded CFS	0.650
	Interface	1.170
S3L200	Bonded CFS	3.120
	Unbonded CFS	2.500
	Interface	1.105
S3L300	Bonded CFS	3.200
	Unbonded CFS	2.542
	Interface	1.086
S5L200	Bonded CFS	5.125
	Unbonded CFS	4.496
	Interface	1.165
S5L300	Bonded CFS	4.363
	Unbonded CFS	4.510
	Interface	1.172

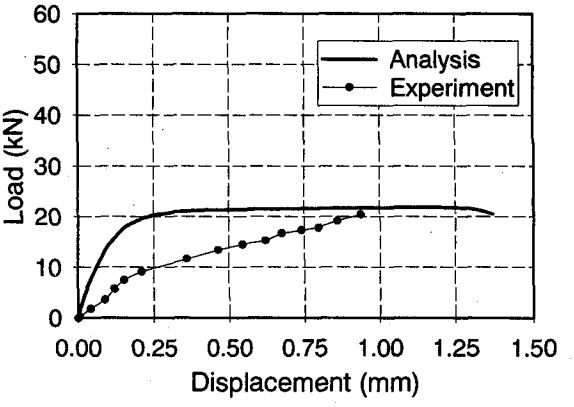

Fig. 10 S1L200 Load - displacement

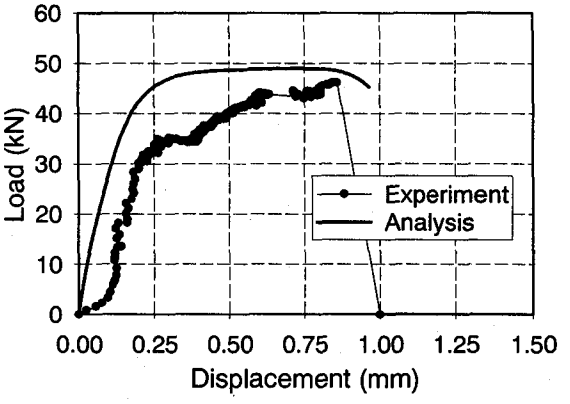

Fig. 11 S3L200 Load - displacement

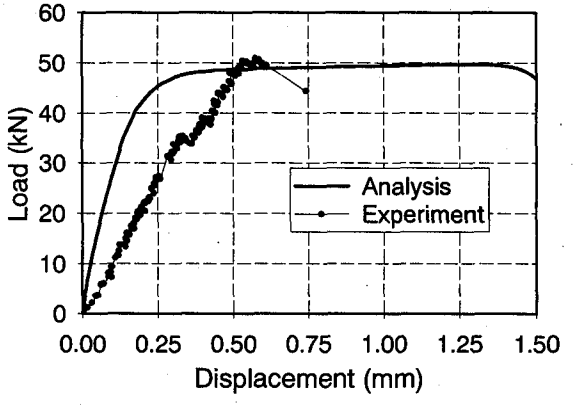

Fig. 12 S3L300 Load - displacement

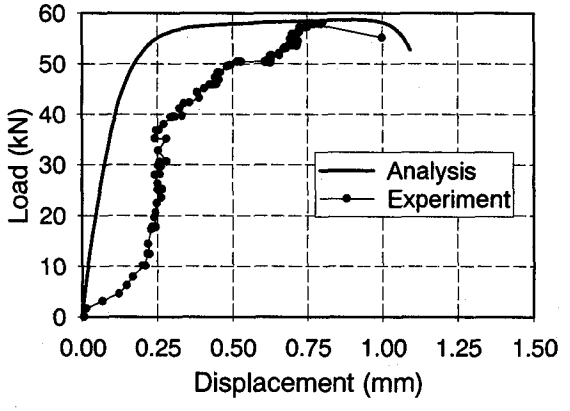

Fig. 13 S5L300 Load - displacement

Table 4 presents the average thickness values for the CFS composite and the interface-bonding layer obtained from the investigation of the pictures similar to the ones presented in Figure 7.

During the experiment, the displacement was measured at the base of the actuator. In order to obtain less error in measurement, the point for which the displacement is plotted is situated at the upper border of the bonded zone. The experimental results were corrected by subtracting the elongation of the unbonded CFS. In addition, the displacement of the concrete block should be subtracted from the remaining displacement also. Unfortunately, the displacement of the concrete block was not available.

From the analytical results of all specimens it was observed that degradation of the shear stiffness of the elements for interface-bonding layer occurred progressively in the direction opposite to the loading direction. The failure mode obtained in the FEM analysis was the complete debonding of the CFS composite.

Due to the inaccurate measurements of the displacements during the loading history the comparison between experiments and FEM analysis for stiffness and displacement can be made only qualitatively.

Figure 10 presents the displacement plotted versus load for specimen S1L200. The peak load measured during the experiment was 20.40kN. The peak load obtained using the FEM was 21.86kN. Figures 12 to 14 present similar plots for specimens S3L200, S3L300 and S5L300, respectively. The peak loads observed during experiment for these specimens were: 46.73kN, 50.82kN, and 58.10kN respectively. The peak loads obtained using the FEM were: 49.02kN, 49.69kN and 58.71kN, respectively. By comparing the values of the peak loads it can be concluded that there is a good agreement between the experiment and analysis results.

By observing the experimental results presented in Figures 10, 11 and 13 it can be seen from the experimental results that the increase in the CFS stiffness causes the increase in the peak load (see also Table 3). The FEM analysis predicts correctly this behaviour.

During the experiments, the displacements at the stage when the debonding area covers almost all the area where the CFS was bonded and when the complete debonding was obtained could not be measured correctly. However, the authors of the experiments reported [13] that the increase of the length of the bonded area caused a larger displacement of the loading point at the failure stage. If the ultimate displacements from Figure 11 and 12 are compared it can be seen that the FEM analysis is able to predict this phenomena.

Figure 14 shows the strain distributions in the CFS composite at different loads, measured along the axis defining the centerline of the specimen S1L200. The upper plot presents the strains measured during the experiment and the lower plot the strains obtained by the FEM analysis respectively. In the experiment, after reaching the load of 20.40kN, the debonding of the CFS composite occurred at a high rate and no further recordings could be done.

Similar plots for specimens S3L300 and S5L300 are presented in Figures 15 and 16, respectively.

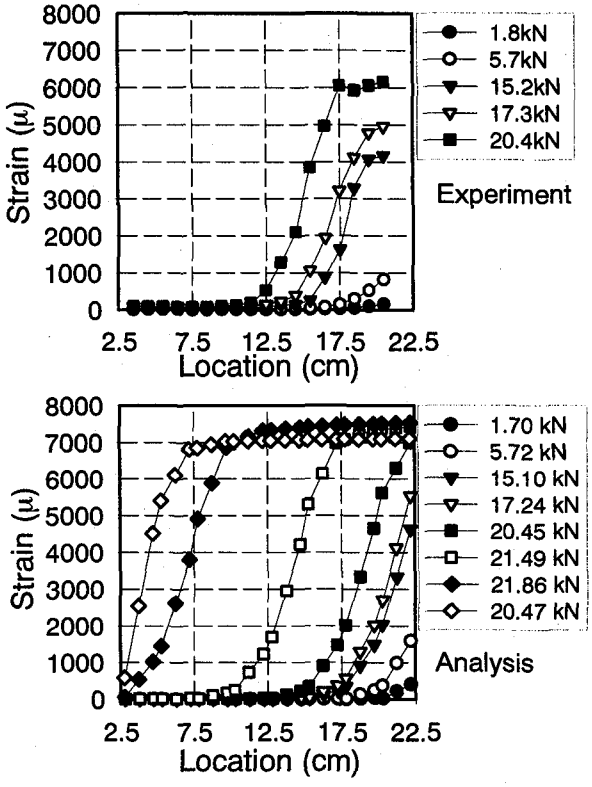

Fig. 14 S1L200 CFS strain distributions

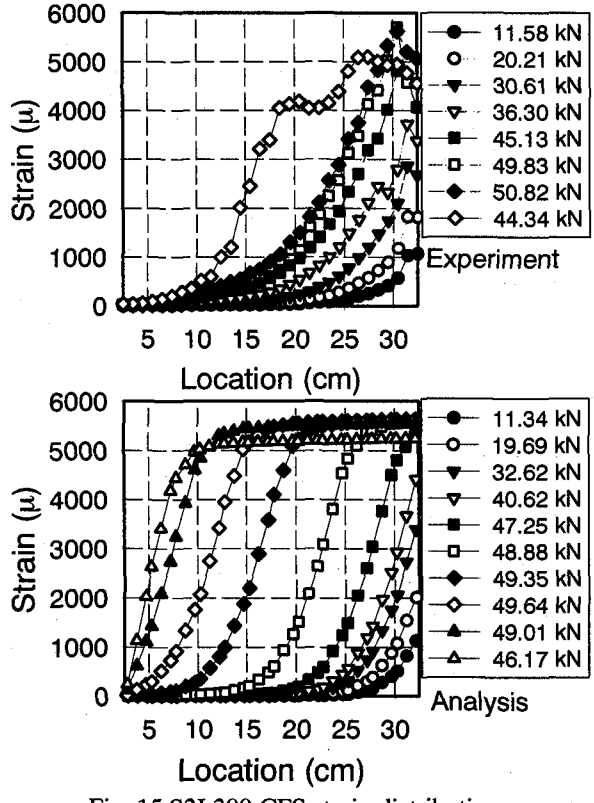

Fig. 15 S3L300 CFS strain distributions

For specimen S3L300, after the 50.82kN load, only one more record could be performed (at 44.34kN) before complete failure. In the case of specimen S5L300 the experiment was performed using a very small step increment and better recordings could be obtained.

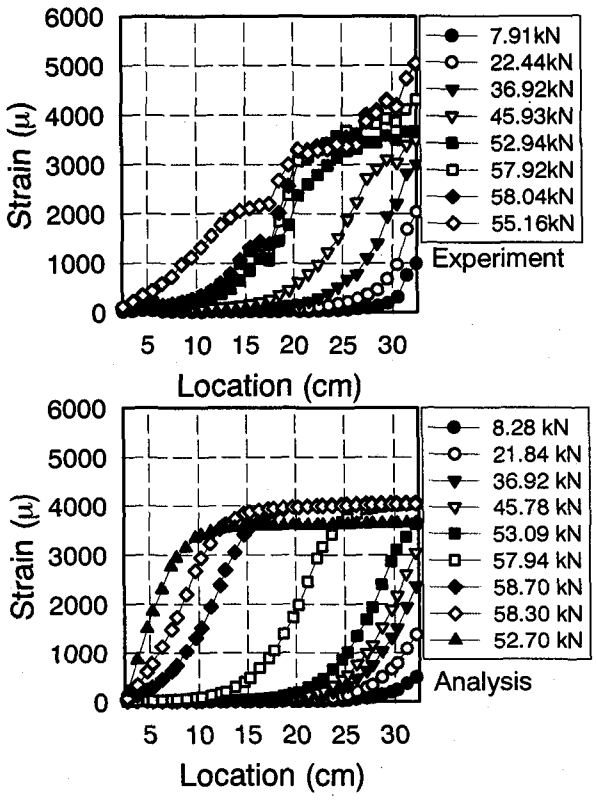

Fig. 16 S5L300 CFS strain distributions

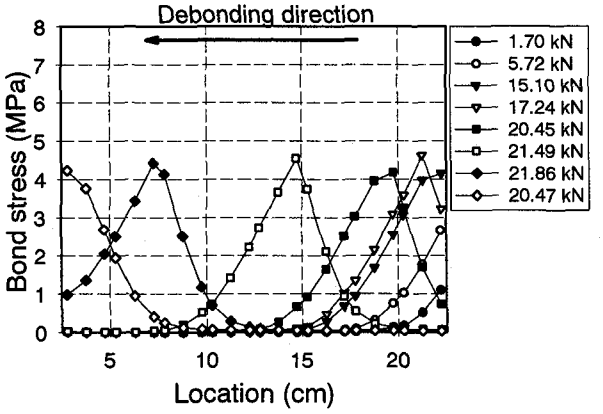

Fig. 17 S1L200 Bond stress distributions in the interface layer - analysis

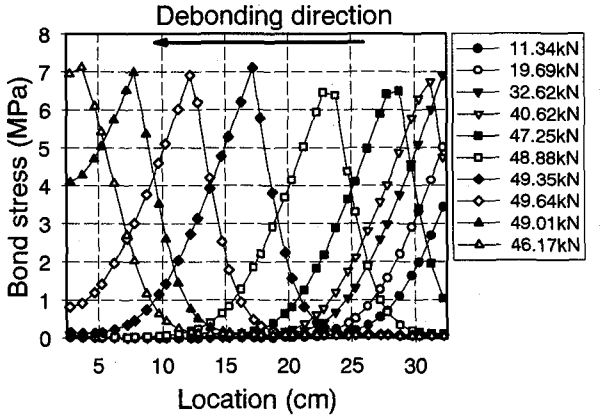

Fig. 18 S3L300 Bond stress distributions in the interface layer - analysis

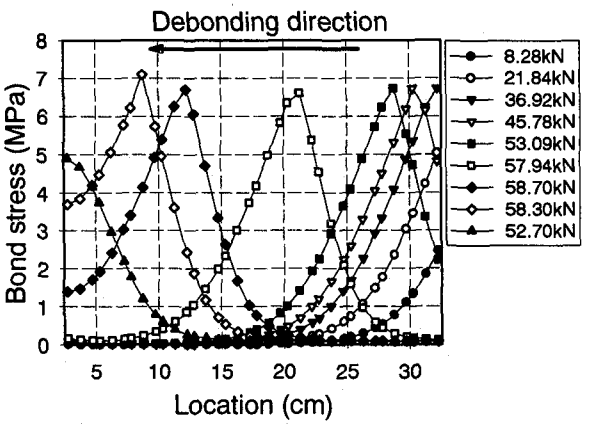

Fig. 19 S5L300 Bond stress distributions in the interface layer - analysis

It can be observed that the maximum strain obtained by the FEM analysis agrees with average maximum strain in the CFS composite recorded during experiments in all three cases presented here. In Figures 14, 15 and 16, the number of layers is increased from 1 to 5. The average maximum strain obtained in CFS decreases from approximately 6000μ to approximately 4000μ. Therefore it can be said that in experiments the increase in CFS composite stiffness, i.e. increase in number of CFS layers, leads to a decrease in the corresponding average maximum strain. The FEM analysis results show the same behaviour.

The maximum strains in CFS obtained by the FEM analysis in the case of one layer agree also with the experimental results presented by Y. Sato et al.[4]. Although the specimens and the setup of experiment are different, comparison of the results obtained in the case of one layer of CFS can be made because the materials characteristics used in experiments are similar.

The average maximum strain in the composite material obtained by Y. Sato. et al.[4] is around 6500μ and the average strain gradient is 168μ/mm (in the zone were the strain increases drastically). The FEM analysis of one layer case carried by the authors indicate a maximum CFS strain of 7000μ and a strain gradient of 129μ/mm for the increasing zone. The strain gradient for specimen S3L300 was 67μ/mm in experiment and 62μ/mm in FEM analysis. For specimen S5L300 the strain gradient was 37μ/mm in the experiment and 42μ/mm in the FEM analysis.

The bond stress and slip relationship used in the FEM analysis is an idealisation of the real relationship (see Figure 1). Therefore, it is most probable that differences in strain distribution in the CFS composite might appear between the experimental and analytical results, as it can be seen from Figures 14, 15 and 16.

Figures 17, 18 and 19 present the bond stress distribution in the interface layer at different loads obtained in the FEM analysis for specimens S1L200, S3L300 and S5L300, respectively. It can be easily observed that as the stiffness of the CFS increases the effective bond length increases also.

The bond stress distribution (FEM results) of the specimen S1L200 presented in Figure 18 agree with the

bond stress observed in experimental results of specimens with one layer of CFS presented by Y. Sato et al.[9].

The increase in peak load from specimen S1L200 to specimen S3L300 is caused by both increases in maximum bond stress value and effective bond length. The difference between the peak loads of specimens S3L300 and S5L300 is caused by the increase of the effective bond length only because the maximum bond stress does not change sensibly.

In reality, the FRP composite can be wrapped and bonded on the structural member (the case of RC columns) or just bonded on the lateral surfaces of the member (RC beams, cantilevers). The proposed method can be applied with no limitation as long as the ultimate load represents the main target for evaluation. At this moment, further study is necessary in order to apply the method in the case when stiffness represents the evaluation target.

5. Conclusions

Application of FRP strengthening methods on reinforced concrete members require analytical tools capable to predict correctly the interfacial stresses developed between the concrete and the FRP composite material.

A new finite element modelling of the interface layer between the CFS composite and concrete was proposed and the analytical results were presented in comparison with the experimental results. Based on the results presented in this paper it can be concluded that:

1) The new finite elements proposed for CFS and interface layer which accommodates precise bond stress-slip relationship, can model the real behaviour of the CFS composite bonded to reinforced concrete elements. A good agreement between experimental and analytical results on peak load and CFS strain distribution was obtained.

2) The results of FEM analysis clearly indicate the effects of CFS stiffness on peak load and CFS strain distribution as observed in experiments.

In the near future, experimental and analytical investigations will be carried out in order to verify the applicability of the newly developed method in a two-dimensional FEM analysis in order to simulate the strengthening effect of the CFS composites bonded on the surface of the RC elements, like cantilever beams or columns, subjected to lateral loads.

Acknowledgements

This study is a part of the research supported by the Japanese Government (Monbusho) scholarship that is greatly acknowledged. The authors are grateful to Dr. Y. Sato from Hokkaido University for his valuable suggestions and advice. The assistance of graduate student W. Moriwaki is also acknowledged. CFS material and epoxy resin were provided by NITTETSU Corporation, Tokyo Japan.

References

1) Malek, A.M. and Saadatmanesh, H., "Physical and Mechanical Properties of Typical Fibers and Resins", *Proc. First Int. Conf. On Composites in Infrastructures*, 1996, Tucson
2) Karbhari, V.M. and Engineer, M, "Investigation of bond between concrete and composites: use of a peel test", *Journal of Reinforced Plastics and Composites*, Vol. 15, pp 208-227, 1996
3) Saadatmanesh, H and Malek, M., "Prediction of shear and peeling stresses at the plate ends of beams strengthened with FRP plates", *Proc. of 3rd Int. Symposium FRPRCS*, Vol. 1, pp 311-318, 1997
4) Yuichi, Sato et al, " Bond behaviour between CFRP sheet and concrete (part 1)", *Journal of Structural and Construction Eng. (Transactions of AIJ)*, Nr. 500, pp 75-82, 1997 (in Japanese)
5) Y. –J. Lee et al, "Tension Stiffening Model for FRP Sheets Bonded to Concrete", *Proc. Second Int. Conf. On Composites in Infrastructures*, pp 175-186, 1998, Tucson
6) Michael J. Chajes et al, "Bond and Force Transfer of Composite Material Plates Bonded to Concrete", *ACI Structural Journal*, March-April, pp 208-217, 1996
7) Yasuhiko Sato et al, "A Study on Prediction of Bond Strength of Continuous Fiber Sheet", *The 6th East Asia-Pacific Conf. On Structural Engineering & Construction*, pp 1319-1324, 1998, Taiwan
8) J. Yin and Z. Wu, " Interface Crack Propagation in Fiber Reinforced Polymer-Strengthened Concrete Structures Using Nonlinear Fracture Mechanics", *ACI SP 188-87*, pp 1035-1047, 1999
9) Yasuhiko Sato et al, "Fundamental study on bond mechanism of Carbon Fiber Sheet", *Journal of Materials, Concrete Structures and Pavements*, No. 648/V-47, May 2000, pp. 71-87 (in Japanese)
10) Yasuhiko Sato et al, "Bond Stress-Slip Relationship of Carbon Fiber Sheet", *Proc. of the 55th Annual Conference of JSCE*, Session V, September 2000 (in Japanese)
11) Hajime Okamura, Koichi Maekawa, "Nonlinear Analysis and Constitutive Models of Reinforced Concrete", ISBN-7655-1506-0 C 3051, 1991
12) Yoshiko Sakai, "Influences of Number of CFS Layers on Bond Fatigue Behaviour of CFS", *Thesis for the Degree of Bachelor of Engineering*, Dept. of Structural and Geotechnical Eng. Hokkaido University, March 1999 (in Japanese)
13) Wataru Moriwaki, "A study on Bond Mechanism of Carbon Fiber Sheet under Cyclic Loading", *Dissertation for the Degree of Master of Science*, Dept. of Structural and Geotechnical Eng. Hokkaido University, March 2000 (in Japanese)

(Received September 14, 2000)